UNIVERSITY OF CALIFORNIA, SAN DIEGO

Image based physiological noise correction for perfusion-based functional MRI

A thesis submitted in partial satisfaction of the requirements for the degree Master of Science

in

Bioengineering

By

Khaled Restom

Committee in charge:

Professor Thomas T. Liu, Chair
Professor Andrew D. McCulloch, Co-Chair
Professor Richard B. Buxton

2004

The Thesis of Khaled Restom is approved by:

_____

_____

_____

_____

_____

University of California, San Diego

2004

DEDICATION

This thesis is dedicated to…..

TABLE OF CONTENTS

LIST OF ABBREVIATIONS

ASL: Arterial Spin Labeling
BOLD: Blood Oxygenation Level Dependent
fMRI: Functional Magnetic Resonance Imaging
GLM: General Linear Model
TR: Repetition Time
CC: Correlation Coefficient
SNR: Signal to Noise Ratio
NMR: Nuclear Magnetic Resonance
CBV: Cerebral Blood Volume
CBF: Cerebral Blood Flow
TE: Echo Time
FOV: Field of View
$CMRO_2$: Cerebral metabolic rate of oxygen
EPI: Echo Planar Imaging

LIST OF FIGURES

LIST OF TABLES

ACKNOWLEDGEMENTS

Thomas T. Liu, PhD.
Richard B. Buxton, PhD
Larry Frank, PhD.
Yashar Behzadi, M.S.
Kamil Uludag, PhD
Yousef Mazaheri, PhD.
Wen-Chau Wu, PhD.
Joanna Perthen, PhD.

ABSTRACT OF THE THESIS

Image based physiological noise correction for perfusion-based functional MRI

By

Khaled S Restom

Master of Science in Bioengineering

University of California, San Diego, 2004

Professor Thomas T. Liu, Chair

Professor Andrew D. McCulloch

Professor Richard B. Buxton

Physiological fluctuations are often a dominant source of noise in functional magnetic resonance imaging (fMRI) experiments, especially at higher field strengths. A number of methods have been developed for the reduction of physiological noise in fMRI experiments. These include image based retrospective correction (RETROICOR), *k*-space based retrospective correction, and navigator echo based correction. At present the application of these methods has been focused primarily on experiments using blood oxygenation level-dependent contrast. Perfusion-based fMRI using arterial spin labeling (ASL) is becoming increasing popular because of its potential to better localize functional activation to the sites of neuronal activity. Thus, in this thesis we investigate four extensions of RETROICOR to ASL. While

significant improvement in statistical power was observed for each method, we found the greatest improvement resulted when 1) physiological noise is estimated separately for tag and control images and 2) the contribution of physiological fluctuations during the tagging process to noise in the tag images is included.

1. INTRODUCTION

Physiological fluctuations are often a dominant source of noise in functional magnetic resonance imaging (fMRI) experiments, especially at higher field strengths {Turner, Jezzard et al. 1993}. Physiological noise in fMRI is manifested as inter-image variation. Since this variance can be on the order of the signal of interest, statistical sensitivity to functional activity can be reduced. Cardiac and respiratory activity have been shown to be the primary sources of physiological noise. Due to the complexity of brain physiology, understanding the contribution of physiological activity to brain imaging remains a challenge.

Cardiac related image intensity fluctuation can be caused by pulsatility of blood flow in the brain, which can result in vessel pulsation, cerebral spinal movement, and tissue deformation. Investigations into the properties of cardiac noise have found that it is largely localized in the brain in regions that are near vessels {Dagli, Ingeholm et al. 1999}. Since MRI is a measure of the magnetization of the imaged tissue, inflow of blood can introduce signal perturbations in parts of tissue near vessels. While this mechanism may explain some of the cardiac related noise, a complete understanding of these effects is lacking.

In addition, Magnetic field fluctuations that result from thoracic cavity expansion and bulk head movement during respiration can also cause undesired image artifacts. In contrast to cardiac related noise, respiratory noise has largely been shown to affect the image globally {Noll and Schneider 1994}. However, localized inter-image

variations around the ventricles and brain edges have also been reported {Glover, Li et al. 2000}.

A number of methods have been developed for the reduction of physiological noise in fMRI experiments. These include image based retrospective correction (RETROICOR) {Glover, Li et al. 2000}, *k*-space based retrospective correction (RETROKCOR) {Hu, Le et al. 1995}, and navigator echo based correction {Pfeuffer, Van de Moortele et al. 2002}. At present the application of these methods has been focused primarily on experiments using blood oxygenation level dependent (BOLD) contrast. However, perfusion-based fMRI using arterial spin labeling (ASL) is becoming increasing popular because of its potential to better localize functional activation to the sites of neuronal activity {Luh, Wong et al. 2000}. In this work we investigate methods for the reduction of physiological noise in ASL experiments. We begin by reviewing the current physiological noise correction methods.

1.1.1 *RETROICOR*

This method assumes that physiological noise induces fluctuation in the MR image time series. Physiological data collected during the imaging sequence used to form a low order Fourier series expansion with cardiac and respiratory phase terms. After the coefficients of the Fourier series are determined by least squares for each pixel time series, the modeled physiological noise is subtracted out. The resultant time exhibits significantly reduced cardiac and respiratory noise {Glover, Li et al. 2000}.

1.1.2 *RETROKCOR*

This method employs the same basic concept as RETROICOR except that the Fourier series is fit to data in the k-space time series, not image space {Hu, Le et al. 1995}. This method showed useful results in correcting respiratory induced effects. However, this method is limited by signal to noise ratio (SNR) and since the SNR is greatest at the center of k-space only time series data near the center of k-space can be fit to the Fourier series. As a result, only low order spatial correction can be made {Glover, Li et al. 2000}.

1.1.3 *Navigator Methods*

Navigator methods use information from an auxiliary echo and the center of k-space of the image to quantify off resonance noise. This method was introduced by Pfeuffer *et al.* as dynamic off-resonance in k-space (DORK) correction {Pfeuffer, Van de Moortele et al. 2002}. The DORK correction method reduces time varying zero and first order phase shifts for EPI imaging. The method assumes that uniform (across each slice) frequency and phase changes result from respiration (due to changes in the magnetic field that cause NMR phase shifts). The phase information is acquired from a navigator echo in addition to data at the center of k-space. Since this method only samples a projection of the brain, it lacks the ability to localize the source of the noise. As a result, its application can result in incomplete correction.

1.1.4 *Estimation of Respiration induced Noise from undersampled multislice fMRI data*

Most fMRI experiments sample brain images at a sampling rate that is the less than the Nyquist frequency for respiratory and cardiac fluctuations. As a result, it is difficult to estimate the contribution of physiological fluctuations since any such contribution will be aliased into lower frequencies. Aliased signals from higher frequency signals can also overlap activity related signals, thereby making it difficult to detect significant activation. The method introduced by Frank et al {Frank, Buxton et al. 2001} uses multislice acquisition to critically sample respiratory induced noise. By reordering the multislice image data using temporal rather than spatial ordering, unaliased respiratory noise is estimated regardless of image repetition time (TR). For example, if 8 slices were acquired in a TR of 2 seconds, the effective slice sampling rate is (2 sec)/(8 slices) = 0.25 sec. Although the pixel time series is sampled at a 2 s TR, reordering the slices temporally (in the order they were acquired) results in a sampling rate that is high enough to sample physiological fluctuations. By detecting global noise in the reordered image time series, this method has been shown to significantly reduce respiratory related noise. However, since cardiac related noise is more localized in the brain image, this method is less successful in reducing cardiac related noise.

1.2 *Application of physiological noise correction to ASL*

Published reports of the application of the current physiological noise correction schemes to ASL have been particularly limited. Among the reviewed correction methods, only DORK has been explicitly used to correct respiratory induced noise in

perfusion fMRI image time series {Pfeuffer, Adriany et al. 2002}. However, a comprehensive description of the application of DORK to ASL was not given.

In this work, we investigate the use of RETROICOR to correct physiological noise in ASL images. Although we had the option to investigate the other reviewed correction schemes, we chose RETROICOR because 1) it required no changes in the MR imaging sequences whereas DORK requires a navigator echo, 2) it provided significant correction of both cardiac and respiratory noise whereas the other correction methods were unsuccessful at removing localized cardiac noise.

1.3 Outline of the thesis

In this thesis, we investigate the use of RETROICOR to correct physiological noise in ASL images. We begin in section 2 with a description of the basics of BOLD and ASL imaging. We then describe the BOLD and ASL general linear model (GLM). Since our perfusion based noise correction methods are based on RETROICOR, it is important that we achieve similar performance in noise correction to that of published results. Consequently, we describe BOLD based physiological noise correction. We then introduce four extensions of RETROICOR to estimate cardiac and respiratory related noise in ASL.

Section 3, describes the imaging and physiological data collection methods. This section will also cover how we assessed the performance of BOLD and ASL correction of physiological noise. We accessed BOLD correction mainly by using similar methods employed in {Glover, Li et al. 2000}, whereas ASL correction was mainly assessed using the F statistic and correlation analysis.

Section 4 presents the results of BOLD and ASL correction of physiological noise. The primary objective of showing the BOLD specific results will be to compare our noise correction results to that of published results in {Glover, Li et al. 2000}. We show that method 4 provided the best improvement in detecting functional perfusion activity.

Section 5 summarizes the results of thesis and discusses the main findings. Finally section 6 suggests area of future work.

Earlier versions of the work presented in this thesis have appeared in {Restom, Behzadi et al. 2004}.

2. THEORY

2.1 BOLD Imaging

BOLD based fMRI has become an indispensable tool for the studies of the working human brain. The BOLD signal reflects local changes in deoxyhemglobin content, and is a complex function of dynamic changes in cerebral blood flow (CBF), cerebral blood volume (CBV), and the cerebral metabolic rate of oxygen ($CMRO_2$), where CBF and $CMRO_2$ are considered to be the variables most directly linked to the neural activity. Although efforts have been developed to estimate this quantities, quantitative interpretation of BOLD fMRI remains difficult {Buxton 2002}.

2.2 Arterial Spin Labeling (ASL)

In contrast to BOLD imaging, ASL has the ability to quantify CBF and also has the potential to better localize brain activity {Luh, Wong et al. 2000}. In an ASL experiment the measured time series is composed of tag images in which the magnetization of inflowing arterial blood is inverted and control images in which the inflowing blood magnetization is relaxed {Detre, Leigh et al. 1992}. Tagging is done with an inversion or saturation RF pulse in a plane that is positioned in a region that is proximal to the imaging slice. The difference between the control and tag images yields an image that is proportional to perfusion {Detre, Leigh et al. 1992}. In contrast to BOLD imaging which uses deoxyhemglobin as a contrast agent, ASL fMRI uses magnetically tagged water as a contrast agent.

2.3 BOLD General Linear Model

In a BOLD weighted fMRI experiment, the measured time series *y[n]* can be modeled as the sum $y[n] = \alpha x[n] + s[n] + p[n] + e[n]$ of a functional activation term comprised of a regressor $x[n]$ with amplitude α, a term *s[n]* representing nuisance terms such as a constant offset and linear drift, a term *p[n]* representing physiological noise, and a term *e[n]* representing additive noise (see Figure 1). For further analysis, it is useful to describe the measured time series with a general linear model (GLM) of the form

$$\mathbf{y} = \mathbf{x}\alpha + \mathbf{Sb} + \mathbf{Pc} + \mathbf{n} \qquad [1]$$

where $\mathbf{y}$ is the $N \times 1$ measurement vector, $\mathbf{x}$ is a $N \times 1$ functional regressor vector, $\mathbf{S}$ is a $N \times l$ matrix comprised of *l* nuisance model functions, $\mathbf{b}$ is an $l \times 1$ vector of nuisance parameters, $\mathbf{P}$ is an $N \times m$ matrix of *m* physiological noise regressors, $\mathbf{c}$ is a $m \times 1$ vector of physiological noise parameters, and $\mathbf{n}$ is a $N \times 1$ additive noise vector with covariance matrix $\sigma^2\mathbf{I}$. To simplify the presentation, we have assumed that the functional regressor is a vector, such as a smoothed boxcar waveform. This is a standard assumption for most block design experiments where the emphasis is on detection of functional activation. We define $\mathbf{x}$ as a smoothed boxcar function, $\mathbf{x} = \mathbf{Xh}$, where $\mathbf{X}$ is a design matrix whose columns are made from shifted versions of the stimulus pattern and $\mathbf{h}$ is the modeled hemodynamic response in vector form. Here we model $\mathbf{h}$ as a the gamma density function of the form

$$h(t) = \begin{cases} 0 & t < \Delta t \\ \dfrac{1}{\tau n!}\left(\dfrac{1}{\tau}\right)^n e^{-t/\tau} & \Delta t \le t \end{cases} \qquad [2]$$

where $n = 3$, $\tau = 1.2s$, $\Delta t = 1s$ {Buxton 2002}. In event-related fMRI experiments where the emphasis is on estimation of the hemodynamic response rather then detecting a response, $\mathbf{h}$ becomes the vector that is solved for in the GLM {Liu, Frank et al. 2001}. Physiological noise correction methods such as RETROICOR estimate the physiological noise regressors either through the use of external physiological measurements or navigator scans. The physiological noise parameters are then estimated from the measured data.

2.3.1 *Noise correction with BOLD general linear model*

The BOLD general linear model can be re-written in the form

$$\mathbf{y} = \mathbf{Z}\mathbf{a} + \mathbf{n} \qquad [3]$$

where $\mathbf{a} = \begin{bmatrix} \alpha & \mathbf{b}^T & \mathbf{c}^T \end{bmatrix}^T$ and $\mathbf{Z} = \begin{bmatrix} \mathbf{x} & \mathbf{S} & \mathbf{P} \end{bmatrix}$. The least squares estimate is $\hat{\mathbf{a}} = \left(\mathbf{Z}^T\mathbf{Z}\right)^{-1}\mathbf{Z}^T\mathbf{y}$. The corrected time series is then given by

$$\hat{\mathbf{y}} = \mathbf{y} - \mathbf{P}\hat{\mathbf{c}} \qquad [4]$$

where $\hat{\mathbf{c}} = \mathbf{A}\hat{\mathbf{a}}$. Here we define $\mathbf{A} = \begin{bmatrix} \mathbf{0}_{1\times(q-r)} & \mathbf{1} \end{bmatrix}$ where q is the number if rows in $\mathbf{a}$ and r is the number of rows in $\mathbf{c}$.

2.4 ASL General Linear Model

The analysis framework we describe in this paper is applicable to arbitrary orderings of tag and control images, but in order to simplify the presentation we assume that the images are interleaved.

To construct the GLM for an ASL experiment, it is useful to introduce the concept of ideal tag and control time series vectors, $\tilde{\mathbf{y}}_{tag}$ and $\tilde{\mathbf{y}}_{con}$, which are defined as the time series that would be obtained if a pair of tag and control images was acquired at every time point [8]. The GLM for these $N \times 1$ vectors is

$$\begin{aligned} \tilde{\mathbf{y}}_{tag} &= \mathbf{x}\alpha_{tag} + \mathbf{S}\mathbf{b}_{tag} + \mathbf{P}_{tag}\mathbf{c}_{tag} + \mathbf{n}_{tag} \\ \tilde{\mathbf{y}}_{con} &= \mathbf{x}\alpha_{con} + \mathbf{S}\mathbf{b}_{con} + \mathbf{P}_{con}\mathbf{c}_{con} + \mathbf{n}_{con} \end{aligned} \quad [5]$$

where the tag and control subscripts reflect the fact that the functional amplitudes, nuisance terms, physiological noise terms, and additive noise may differ between the tag and control states. In addition, the number of physiological noise regressors may differ for the tag versus control states, so that $\mathbf{P}_{tag}$ and $\mathbf{P}_{con}$ may have different dimensions. We model the interleaving process by multiplying the ideal vectors by downsampling matrices to obtain the measured tag and control time series

$$\begin{aligned} \mathbf{y}_{tag} &= \mathbf{D}_{tag}\tilde{\mathbf{y}}_{tag} = \mathbf{D}_{tag}\mathbf{y} \\ \mathbf{y}_{con} &= \mathbf{D}_{con}\tilde{\mathbf{y}}_{con} = \mathbf{D}_{con}\mathbf{y} \end{aligned} \quad [6]$$

where $\mathbf{D}_{tag}$ and $\mathbf{D}_{con}$ are $p \times N$ downsampling matrices that pick out every even sample and odd sample, respectively, and $p = N/2$. Equations 5 and 6 may be combined to yield

$$\begin{bmatrix} \mathbf{y}_{tag} \\ \mathbf{y}_{tag} \end{bmatrix} = \begin{bmatrix} \mathbf{D}_{tag}\mathbf{x} & \mathbf{0} \\ \mathbf{0} & \mathbf{D}_{con}\mathbf{x} \end{bmatrix} \begin{bmatrix} \alpha_{tag} \\ \alpha_{con} \end{bmatrix} + \begin{bmatrix} \mathbf{S}' & \mathbf{0} \\ \mathbf{0} & \mathbf{S}' \end{bmatrix} \begin{bmatrix} \mathbf{b}_{tag} \\ \mathbf{b}_{con} \end{bmatrix} + \begin{bmatrix} \mathbf{D}_{tag}\mathbf{P}_{tag} & \mathbf{0} \\ \mathbf{0} & \mathbf{D}_{con}\mathbf{P}_{con} \end{bmatrix} \begin{bmatrix} \mathbf{c}_{tag} \\ \mathbf{c}_{con} \end{bmatrix} + \mathbf{n} \quad [7]$$

where we have made the reasonable approximation that the downsampled nuisance matrices $\mathbf{D}_{tag}\mathbf{S}$ and $\mathbf{D}_{con}\mathbf{S}$ span the same space and can thus be replaced by a single matrix $\mathbf{S}'$.

2.5 Noise Correction with the ASL General Linear Model

In this thesis, we examine the effect of different assumptions about $\mathbf{P}_{tag}$, $\mathbf{P}_{con}$, $\mathbf{c}_{tag}$, and $\mathbf{c}_{con}$ on the physiological noise removal process. In the most obvious application of RETROICOR to an ASL experiment, we assume that the physiological noise regressors and parameters are the same for both tag and control images. This is equivalent to setting $\mathbf{P}_{tag} = \mathbf{P}_{con} = \mathbf{P}$ and $\mathbf{c}_{tag} = \mathbf{c}_{con}$. The next level of complexity is to assume that the physiological noise regressors are the same but that the parameters can differ, i.e. $\mathbf{c}_{tag} \neq \mathbf{c}_{con}$. We refer to noise correction with these two sets of assumptions as Methods 1 and 2.

The physiological noise regressor matrix $\mathbf{P}$ for methods 1 and 2 accounts for the impact of physiological variations on the acquisition of the image. In an ASL experiment, we hypothesize that there may be an additional effect of these variations on the tagging process. For example, the efficiency of the magnetic inversion can depend on the velocity of blood in the tagging region, and can therefore be affected by cardiac pulsations. To model this effect, we expand $\mathbf{P}_{tag}$ to include a matrix $\mathbf{P}'$ of regressors reflecting the physiological parameters at a time that is ΔT seconds prior to the image acquisition, so that $\mathbf{P}_{tag} = \left[\mathbf{P} \quad \mathbf{P}'\right]$. For a standard ASL experiment, we

would expect ΔT to be near the inversion time *TI* of the experiment. For a quantitative ASL experiment (e.g. QUIPSS II) {Wong, Buxton et al. 1998} with additional post-inversion saturation pulses, we would expect ΔT to lie between the inversion time TI_2 and the saturation time $TI_2 - TI_1$, i.e. $(TI_2 - TI_1) \le \Delta T \le TI_2$.

We define methods 3 and 4 as extensions of methods 1 and 2, respectively, with the expanded $\mathbf{P}_{tag}$ matrix. In method 3, the physiological noise is assumed to affect the tag and control image acquisitions equally, with an additional set of parameters to reflect the effect on the tagging process, so that $\mathbf{c}_{tag} = \begin{bmatrix} \mathbf{c}_{con}^T & \bar{\mathbf{c}}_{tag}^T \end{bmatrix}^T$ where $\bar{\mathbf{c}}_{tag}$ is the vector of parameters for the regressors in $\mathbf{P}'$. For method 4, the noise can affect the tag and control image acquisitions independently, so that $\mathbf{c}_{tag} = \begin{bmatrix} \tilde{\mathbf{c}}_{tag}^T & \bar{\mathbf{c}}_{tag}^T \end{bmatrix}^T$ where $\tilde{\mathbf{c}}_{tag} \neq \mathbf{c}_{con}$.

The general linear model for each of the four methods can be written as

$$\tilde{\mathbf{y}} = \mathbf{Z}\mathbf{a} + \mathbf{n} \qquad [8]$$

where $\tilde{\mathbf{y}} = \begin{bmatrix} \mathbf{y}_{tag}^T & \mathbf{y}_{con}^T \end{bmatrix}^T$; $\mathbf{a} = \begin{bmatrix} \alpha_{tag} & \alpha_{con} & \mathbf{b}_{tag}^T & \mathbf{b}_{con}^T & \mathbf{c}_{TOT}^T \end{bmatrix}^T$;

$\mathbf{Z} = \begin{bmatrix} \mathbf{X} & \mathbf{S}_{TOT} & \mathbf{P}_{TOT} \end{bmatrix}$ with $\mathbf{X} = \begin{bmatrix} \mathbf{D}_{tag}\mathbf{x} & \mathbf{0} \\ \mathbf{0} & \mathbf{D}_{con}\mathbf{x} \end{bmatrix}$, $\mathbf{S}_{TOT} = \begin{bmatrix} \mathbf{S}' & \mathbf{0} \\ \mathbf{0} & \mathbf{S}' \end{bmatrix}$, and $\mathbf{P}_{TOT}$ and $\mathbf{c}_{TOT}$ for each method are defined in Table 1. An illustrative summary of all four methods is shown in figure 2.

The statistical significance of functional perfusion activation is assessed by testing whether the difference $\alpha_{con} - \alpha_{tag}$ of the control and tag amplitudes is significantly different from zero. This can be accomplished with an F-statistic of the form

$$F = (N-q)\frac{\hat{\mathbf{a}}^T\mathbf{A}^T\left(\mathbf{A}\left(\mathbf{Z}^T\mathbf{Z}\right)^{-1}\mathbf{A}^T\right)\mathbf{A}\hat{\mathbf{a}}}{\left(\tilde{\mathbf{y}}-\mathbf{Z}\hat{\mathbf{a}}\right)^T\left(\tilde{\mathbf{y}}-\mathbf{Z}\hat{\mathbf{a}}\right)} \quad [9]$$

where $\hat{\mathbf{a}} = \left(\mathbf{Z}^T\mathbf{Z}\right)^{-1}\mathbf{Z}^T\tilde{\mathbf{y}}$; $\mathbf{A} = \begin{bmatrix}-1 & 1 & \mathbf{0}_{1\times(q-2)}\end{bmatrix}$; and q is the number of rows in $\mathbf{a}$.

The F-statistic has the useful property of explicitly taking into account the reduced degrees of freedom due to adding more physiological noise terms {Liu, Wong et al. 2002}.

2.6 Physiological Noise Model

The matrix $\mathbf{P}$ is composed of physiological noise regressors. As defined in {Glover, Li et al. 2000}, the nth row of the matrix is given by:

$$\begin{bmatrix}\cos(C_n) & \cos(2C_n) & \sin(C_n) & \sin(2C_n) & \cos(R_n) & \cos(2R_n) & \sin(R_n) & \sin(2R_n)\end{bmatrix} \quad [10]$$

where $C_n = \varphi_c[n]$ is the cardiac phase, $R_n = \varphi_r[n]$ is the respiratory phase, and n indexes the image data acquired at time $t = nTR$. The columns of $\mathbf{P}$ thus form the terms for a 2nd order Fourier series expanded out in terms of cardiac (columns 1-4) and a 2nd order Fourier series expanded out in terms of respiratory phase (columns 5-6).

To motivate the use of a Fourier expansion, it useful to look at the cardiac cycle as an example. Although the time interval between consecutive heartbeats may differ

during the experiment, each signal change is assumed to be related to the phase of the cardiac cycle. However, since the cardiac signal is measured at the index finger, resultant signal changes in brain voxels may be time shifted to the cardiac phase. A Fourier series expansion allows for this time shift to be estimated on a per-voxel basis. It has been reported that a 2nd order Fourier expansion is sufficient physiological noise estimation {Glover, Li et al. 2000}.

Following Hu {Hu, Le et al. 1995}, cardiac phase is defined as

$$\varphi_c[n] = 2\pi \frac{t - t_1}{t_2 - t_1} \qquad [11]$$

where t is the time at which the image is acquired, t_1 is the time of the cardiac peak immediately prior to t, and t_2 is the time of the cardiac peak immediately following t. Assuming that the cardiac phase advances linearly, this method scales the cardiac signal to a number between 0 and 2π {Glover, Li et al. 2000}. Example data showing the calculation of cardiac phase are shown in figure 3.

Respiratory phase is presented as

$$\varphi_r[n] = \pi \frac{\sum_{b=1}^{rnd(\frac{R[t]}{R_{\max}} \cdot 100)} H[b]}{\sum_{b=1}^{100} H[b]} \operatorname{sgn}(dR/dt) \qquad [12]$$

where rnd denotes a integer rounding operation, $R[t]$ is the amplitude of the signal from the respiratory belt normalized from 0 to $R_{\max}$ (maximum of $R[t]$), and $H[b]$ is a histogram of the number of occurrences of respiratory amplitude values that occur at bin value b. Bin values span $0.01R_{\max}$ thru $R_{\max}$ with intervals of $0.01(b)(R_{\max})$.

The term $\mathrm{sgn}(dR/dt)$ is the sign of dR/dt, with a value of 1 during inspiration and –1 during exhalation. To calculate $\mathrm{sgn}(dR/dt)$, we used a sliding window that spans two consecutive respiratory signal peaks. A value of -1 is given to all data points preceding the minimum data point, whereas a value of +1 is given to the rest of the points within the window. This process is continued for each succeeding window. When the $\mathrm{sgn}(dR/dt)$ value is positive (inhalation), $\varphi_r[n]$ spans 0 to π, whereas when $\mathrm{sgn}(dR/dt)$ is negative (exhalation), $\varphi_r[n]$ is negated. This method assumes that B_0 fluctuation are proportional to the extent of inhaling or exhaling rather than the onset of max inspiration {Glover, Li et al. 2000}. Example data showing the calculation of respiratory phase are presented in figure 4.

3. METHODS

3.1 Imaging

Four healthy adult male volunteers participated as subjects in this study. All experimental imaging data were collected on a Varian 4T whole body system with head transmit coil and a surface receive coil (Nova Medical) placed under the occipital lobe. Three oblique 8mm slices through the calcarine sulcus were imaged while the subject was shown a full-field, 8 Hz radial flickering checkerboard (block design comprised of 4 periods of 30/30 seconds on/off). ASL data were acquired using a PICORE-QUIPSS II {Wong, Buxton et al. 1998} sequence with an echo planer imaging (EPI) readout, interleaving of tag and control images, and TR = 2s, repetitions = 130, TI1/TI2 = 700/1400 ms, TE = 27 ms, θ = 90, FOV 24cm, 64x64 matrix. BOLD-weighted resting state data were acquired using an echo planar sequence with TR =250 ms, repetitions = 1040, TE = 27 ms, θ = 90, FOV 24cm, and 64x64 matrix. Image data were co-registered to minimize the effects of subject motion {Cox 1996}.

3.2 Physiological Data Collection

Cardiac pulse and respiratory effort data were monitored using a pulse oximeter (NONIN) and a respiratory effort transducer (BIOPAC), respectively. The pulse oximeter was placed on the subject's right index finger. The respiratory effort belt was placed around the subject's abdomen. Physiological data were sampled at 40 samples per second using a multi-channel data acquisition board (National

Instruments). In addition to the physiological data, scanner TTL pulse data (10 ms duration, 5 volt pulse per slice acquisition) were recorded at 1 kHz. The TTL pulse data were used to synchronize the physiological data to the acquired images.

3.3 Data Analysis

3.3.1 *BOLD weighted images*

The RETROICOR algorithm as described in section 2 was applied to the resting state BOLD data acquired at a TR of 250 ms. To assess the overall effectiveness of the algorithm, the standard deviation in each voxel was computed for the resting state times series before and after noise correction. In addition, the power spectrum of each time series was computed and the average spectral energies in 0.1 Hz frequency bands around the respiratory peak and the cardiac peak were calculated. Respiratory and cardiac peaks ranged between 0.2 to 0.4 Hz and 0.9 to 1.1 Hz, respectively, across subjects. To evaluate the performance of RETROICOR with a TR more similar to that used in typical fMRI studies, the TR = 250 ms BOLD data were downsampled to form time series with a TR of 2000 ms. These downsampled data were then analyzed in a manner similar to the original data.

3.3.2 *Perfusion weighted images*

In order to assess the relative performance of the different methods, the F-statistic was computed for a general linear model in which $\mathbf{x}$ (as defined in section 2.3) is treated as the regressor of interest and the physiological noise terms are treated as

nuisance terms {Liu, Wong et al. 2002}. In addition, zeroth and first order Legendre polynomials are included as constant and linear nuisance terms.

F-statistics for methods 1 through 4 described in section 2.5 were calculated for each pixel within a region of interest (ROI) defined to encompass the visual cortex. To determine the optimal delay Δ to use with methods 3 and 4, the F-statistic was calculated at delay times varying between 0 s to 1.5 s at intervals of 25ms for uncorrected pixels that showed significant perfusion ($p < 0.05$). The optimal Δ's for method 3 and 4 were chosen to maximize the average F-statistic over each slice.

To compare the performance of each method, we evaluated the number of pixels that exceeded a range of threshold F statistic value. The threshold F statistic values corresponded to p values ranging from 0.00 to 0.05. These were calculated for each method and the uncorrected data.

Since correlation analysis is often used in fMRI {Buxton 2002}, we also evaluated each of the noise correction methods by calculating correlation coefficients. For each voxel, a perfusion time series was computed from the running difference of control and tag images {Wong, Buxton et al. 1997} both prior to and after noise correction. These time series were then correlated with a smoothed boxcar reference function defined in section 2.3.

4. RESULTS

4.1 BOLD data

Example data showing estimated cardiac and respiratory components from on voxel of the short TR BOLD data are shown in figure 5. To compare the estimated cardiac and respiratory components to the measured physiological signal during the experiment, both measured cardiac and respiratory signals (downsampled to 4 Hz) are also shown. The estimated respiratory component is similar to the measured signal. There is a delay between the measured cardiac signal and the estimated cardiac component. This delay is on the order of 0.4 s.

Respiratory and cardiac-related spectral components of the short TR BOLD data are shown in figures 6 and 7, respectively. The data shown are for subject 1, with similar results seen for the other subjects. Both respiratory and cardiac components were significantly attenuated by the RETROICOR algorithm. Cardiac components are extensively localized to gray matter sulci and regions near large vessels, whereas respiratory components are primarily located on the brain edges. Figures 8 and 9 show an example Fourier spectrum and time series, respectively, from a selected voxel. As shown by Figure 8a, the application of the RETROICOR algorithm clearly reduces both cardiac and respiratory related components. For reference, the spectra of the measured physiological data are also shown in 8b and 8c. The corrected time series in Figure 9 shows a 30% reduction in the standard deviation as compared to the uncorrected time series.

Spectral component images and example spectra for the resampled BOLD data (TR = 2000 ms) are shown in Figures 10 and 11, respectively. Figure 10 is analogous to figures 6 and 7 for the short TR data. However, since the cardiac components are aliased into the range that overlaps the respiratory frequency band, only one figure is shown. The difference images shown in the third column of figure 10 show a significant reduction in localized regions such as gray matter sulci along the brain edges. The example Fourier spectrum in figure 11 demonstrates a clear reduction of the physiological components. Physiological data resampled to the 0.5 Hz image sampling rate (second row in Figure 11) show that the cardiac component aliases down to the same frequency range as the respiratory components. Consistent with the data shown in figure 9, the corrected time series in Figure 12 shows a 30% reduction in the standard deviation as compared to the uncorrected long TR data.

4.2 ASL data results

F statistics were assessed for delay ranging from 0 ms to 1500 ms. Results shown in figure 13 are for subject 1. Method 4 was used as the mode of correction when searching for the optimal delay time Δ, with similar results observed for method 3. The average F statistic of ROI (section 3.3.2) peaked at delay times of 850 ms, 900 ms and 950 ms for slices 1, 2, and 3, respectively. Slice to slice delay time differences are consistent with the image acquisition delay of 50 ms. To show that the results are similar across subjects, figure 14 shows data averaged over all subjects. The observed time to peak is consistent with that observed for subject 1. A summary of the delay times used with methods 3 and 4 are shown in Table 2.

To compare the proposed methods, Figure 15 shows the number of voxels (within an ROI) that have an F-statistic above a threshold corresponding to p-values between 0 and 0.05. For any given p value, method 4 provided the largest number of significant voxels. It is also worth noting that method 3 is an improvement over method 1, indicating that the improvement due to the addition of the delay term is consistent for both methods 1 and 2. The average performance over all subjects is shown in figure 16. The results are consistent with those for subject 1.

To show the level of correction achieved by method 4, an example perfusion time series is shown in figure 17 for subject 1. The selected voxel shown was chosen to show the greatest degree of correlation improvement. Upon visual examination of the two perfusion time series, functional activation is clearly difficult to detect prior to correction. The correlation maps of slice 1 for this subject were also significantly improved by method 4, as shown in figure 18. Additional voxels that exceeded the set threshold after correction remained localized in a region that encompasses the visual cortical gray matter. To compare the performance of the proposed methods in terms of the number of correlated voxels, figure 19 is a bar graph which shows the mean number of voxels across subjects that exceed the threshold of 0.4. Consistent with the results in indicated in figure 16, method 4 provided the greatest improvement in correlated voxels.

5. DISCUSSION

5.1 BOLD weighted imaging

As evidenced in figures 6, 7, and 10, cardiac and respiratory related noise have certain spatial characteristics. Cardiac related spectral energy is localized to gray matter sulci and regions that are close to large vessels such as the sagittal sinus. Since regions made up of primarily gray matter have a higher concentration of blood vessels, we expect the impact of cardiac pulsatility to be greatest in gray matter regions. Respiratory related noise, on the other hand, seems to be localized to the outer edges of the brain. This effect may be caused by the occurrence of bulk head movement during respiration.

The performance we achieved in BOLD imaging correction is quantitatively similar to that published in {Glover, Li et al. 2000}. We achieved a reduction in cardiac and respiratory spectral components in both short and long TR BOLD imaging that is comparable to the published results. Additionally, results in {Glover, Li et al. 2000} report a 35% decrease in the standard deviation of long TR BOLD data after correction. This is comparable to the 30% decrease that we report.

5.2 Perfusion weighted imaging

The observed improvement of method 2 when compared to method 1 is the first main finding of this thesis. This indicates that physiological noise should be estimated for tag and control images separately. In other words, the amplitude of physiological noise in tag images is different than that of control images. Referring to the GLM

described in section 2.5, this observation indicates that allowing for $\mathbf{c}_{tag} \neq \mathbf{c}_{con}$ is an important first step when estimating physiological noise in ASL.

The second main finding is that method 4 provided the greatest degree of physiological noise correction. This observation supports the assumption behind methods 3 and 4, mainly that the process of tagging blood can be modulated by cardiac and respiratory activity. In addition, the observed optimal delay time Δ is consistent with the temporal range of the arterial bolus created by the QUIPPS II pulse sequence.

6. AREAS OF FUTURE WORK

Since tag images were found to effected by physiological noise differently than control images, it would be interesting to resolve the source of the noise. Based on the ASL sequence we used, the effective TR between tag images is 4 s. Due to aliasing of respiratory and cardiac components, this TR is clearly too high to resolve differences between cardiac and respiratory effects. One possible method to resolve these differences would be to acquire only tag images at the shortest TR possible. However, a shorter TR is limited by transit delay times between the tagged bolus and its arrival to the imaging region. If we assume that tagged blood arrives at the larger vessels fast enough, then it may be possible to have a TR that is on the order of 300 ms. In addition, if the tagging process is modulated by cardiac and respiratory activity, a shorter TR may resolve whether cardiac pulsatility or respiratory modulation of the magnetic field has greater effect.

Overall, this thesis has treated cardiac and respiratory effects as noise. An alternative approach to treating cardiac and respiratory effects as noise would be to treat these effects as signals of interest. Combining these signals with other fMRI data such as CBF, CBV, and $CMRO_2$ signals may yield new light onto the understanding of brain physiology.

APPENDIX A: TABLES

Method	Assumptions	$\mathbf{P}_{TOT}$	$\mathbf{c}_{TOT}$
1	Identical noise parameters for tag and control image acquisitions.	$\begin{bmatrix} \mathbf{D}_{tag}\mathbf{P} \\ \mathbf{D}_{con}\mathbf{P} \end{bmatrix}$	$\mathbf{c}_{tag}$
2	Different noise parameters for tag and control image acquisitions	$\begin{bmatrix} \mathbf{D}_{tag}\mathbf{P} & \mathbf{0} \\ \mathbf{0} & \mathbf{D}_{tag}\mathbf{P} \end{bmatrix}$	$\begin{bmatrix} \mathbf{c}_{tag} \\ \mathbf{c}_{con} \end{bmatrix}$
3	Method 1 with addition of noise during tagging process.	$\begin{bmatrix} \mathbf{D}_{tag}\mathbf{P} & \mathbf{D}_{tag}\mathbf{P}' \\ \mathbf{D}_{con}\mathbf{P} & \mathbf{0} \end{bmatrix}$	$\begin{bmatrix} \mathbf{c}_{tag} \\ \bar{\mathbf{c}}_{tag} \end{bmatrix}$
4	Method 2 with addition of noise during tagging process	$\begin{bmatrix} \mathbf{D}_{tag}\mathbf{P} & \mathbf{D}_{tag}\mathbf{P}' & \mathbf{0} \\ \mathbf{0} & \mathbf{0} & \mathbf{D}_{con}\mathbf{P} \end{bmatrix}$	$\begin{bmatrix} \tilde{\mathbf{c}}_{tag} \\ \bar{\mathbf{c}}_{tag} \\ \mathbf{c}_{con} \end{bmatrix}$

Table 1. Summary of physiological noise regressors ($\mathbf{P}_{TOT}$) and physiological noise parameters ($\mathbf{c}_{TOT}$)

	Delay time (Δ) in ms		
Subject	**Slice 1**	**Slice 2**	**Slice 3**
1	850	900	950
2	825	875	925
3	775	825	875
4	825	875	925

Table 2. Summary of estimated delay times (Δ) that were used with methods 3 and 4

APPENDIX B: FIGURES

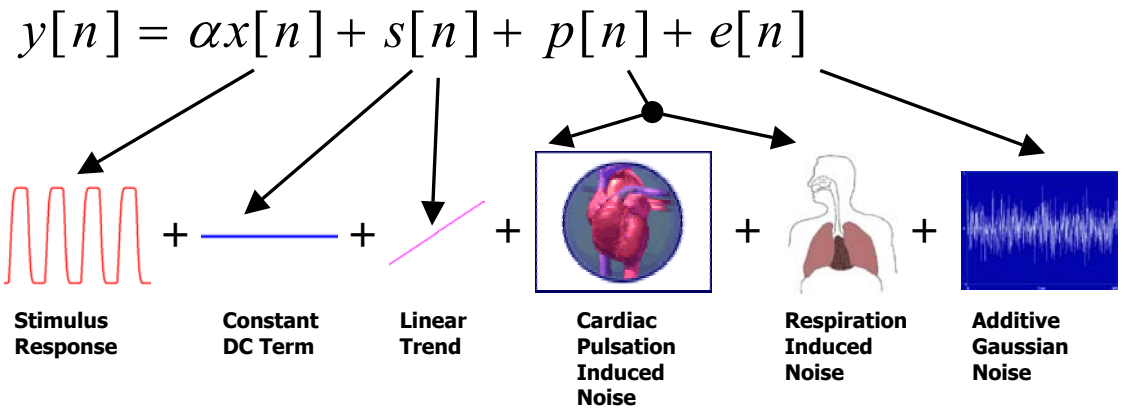

Figure 1. Pixel signal model (Section 2.3)

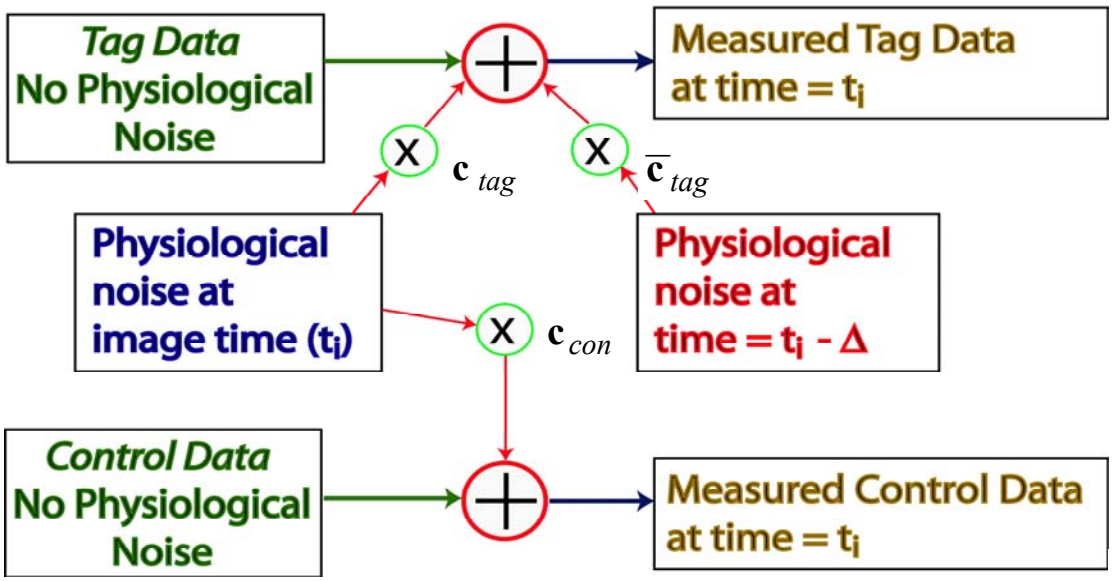

Figure 2. A simplified model of an ASL experiment. The measured tag and control images are assumed to be the sum of a noiseless image plus the physiological noise occurring at image acquisition time t_i. The relative impact of the physiological noise on tag and control image acquisition is modeled by the constants $\mathbf{c}_{tag}$ and $\mathbf{c}_{con}$, respectively. The possible effects of cardiac pulsations and respiration on the inversion process are included in the additional term for physiological noise at time $t_i - \Delta$ with a weight $\bar{\mathbf{c}}_{tag}$. In applying RETROICOR to ASL data, we consider 4 possible methods. In method 1 we assume that the noise affects the tag and control images equally ($\mathbf{c}_{tag} = \mathbf{c}_{con}$) and there is no delayed tag term ($\bar{\mathbf{c}}_{tag} = \mathbf{0}$). This can be considered to be the direct application of RETROICOR to ASL. Method 2 allows for the possibility that the noise affects the tag and control images differently ($\mathbf{c}_{tag} \neq \mathbf{c}_{con}$), while methods 3 and 4 are modified versions of 1 and 2, respectively, that include a delayed tag term ($\bar{\mathbf{c}}_{tag} \neq \mathbf{0}$).

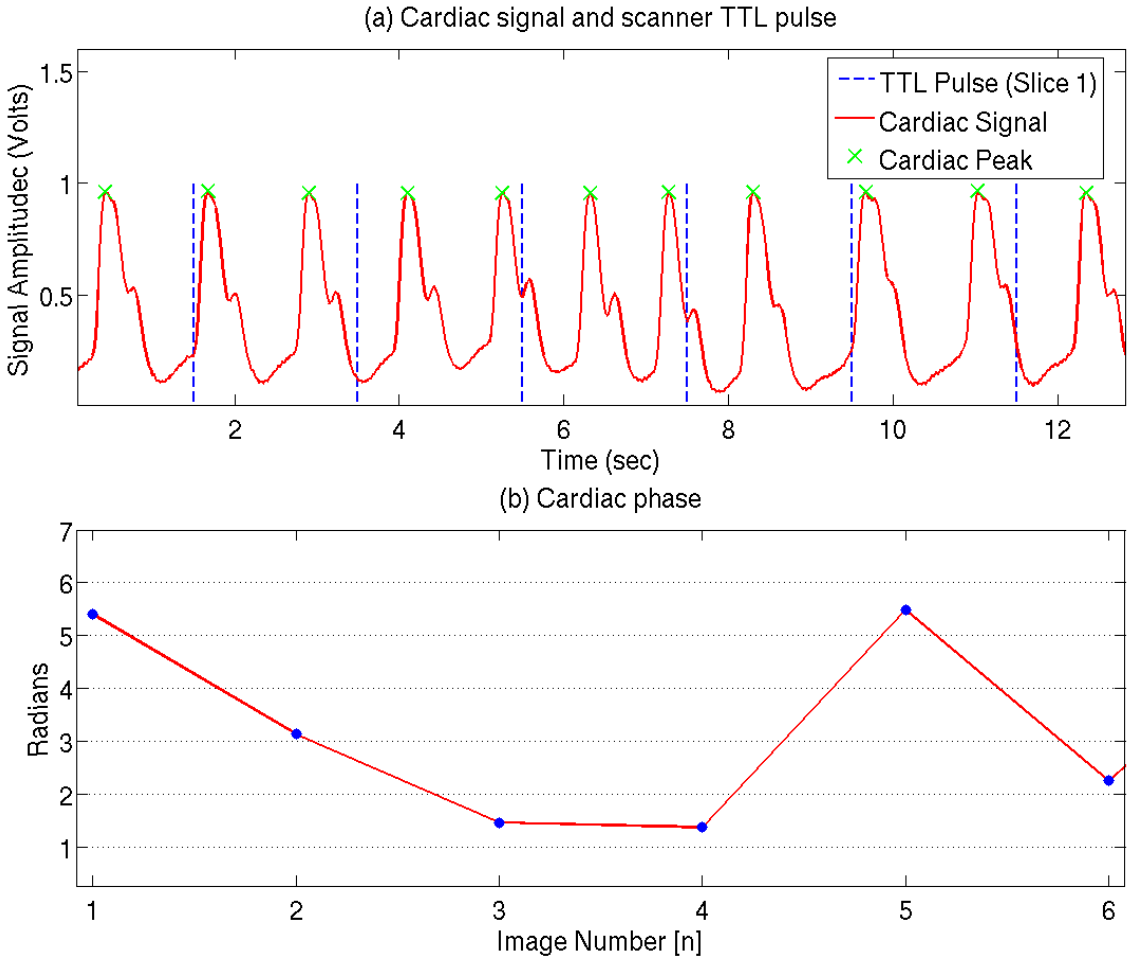

Figure 3. Example showing calculation of cardiac phase (b). Peak of the cardiac cycle is denoted by a green x in (a). Calculation of cardiac phase for image number 3 is explained as follows: The 3rd TTL pulse shown in (a) corresponds to image number 3. The difference between the time that image 3 is sampled and the time of the preceding cardiac peak is approximately 0.3 sec. The difference in time between this cardiac peak and the following cardiac peak is approximately 1.2 sec. Referring to equation 11, cardiac phase at image 3 equates to

$$\varphi_c[3] = 2\pi \frac{0.3}{1.2} = 1.4$$

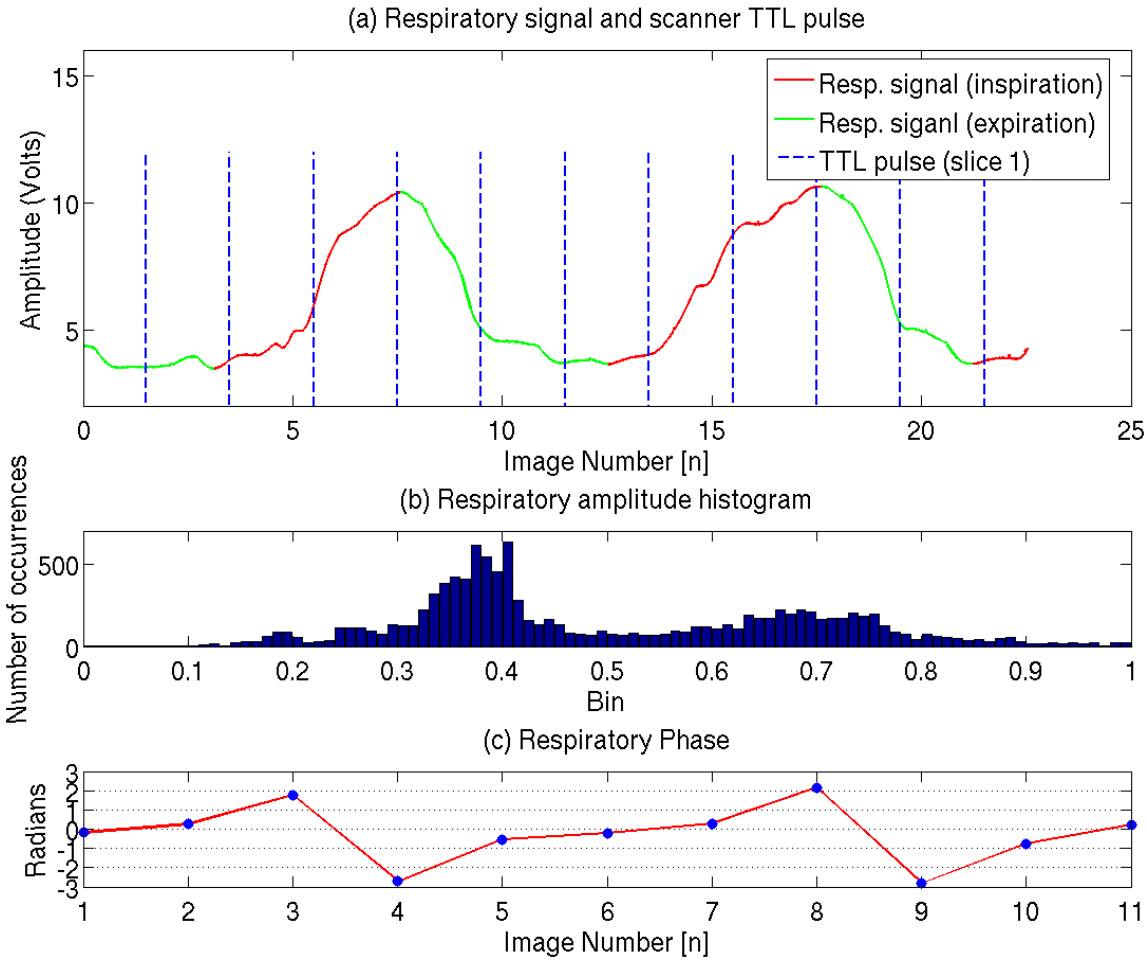

Figure 4. Example showing calculation of respiratory phase (c). Peak respiratory activity shown in (a) is roughly 80 % of maximum respiration during the collected time series. Respiratory amplitude histogram is shown in (b). Bin values in (b) span $0.01R_{\max}$ thru $R_{\max}$ with intervals of $0.01R_{\max}$. Calculation of respiratory phase for image number 3 is explained as follows: The 3rd TTL pulse shown in (a) corresponds to image number 3. The respiratory activity during image 3 is 50% of maximum respiration during the imaging experiment. The number of occurrences in bin values from 0.01 to 0.50 is 6704. The sum of all occurrences is 11204. $\mathrm{sgn}(dR/dt)$ is positive. Referring to equation 12, respiratory phase at image number 3 is

$$\varphi_r[3] = \pi \frac{6704}{11204} = 1.9$$

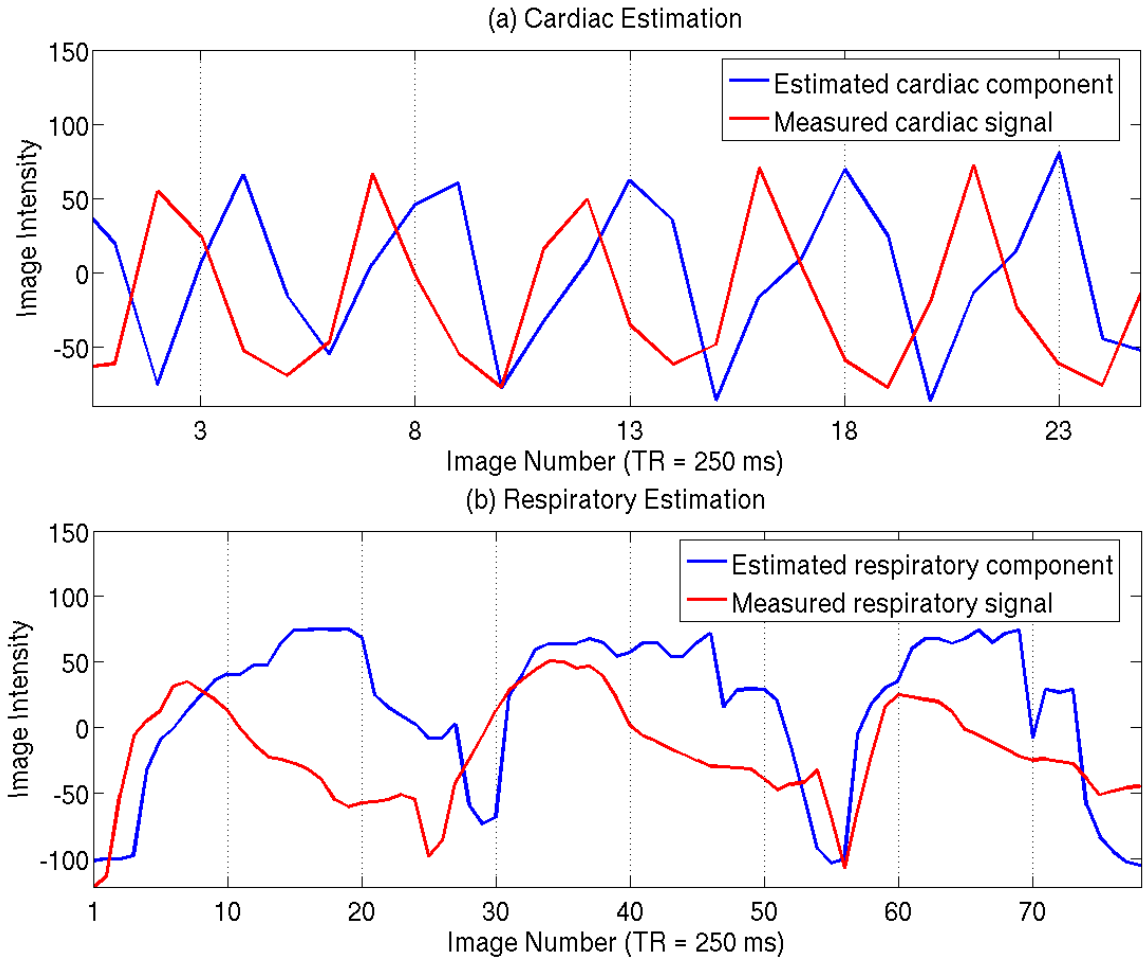

Figure 5. Example data from one voxel showing estimated (a) cardiac and (b) respiratory components estimated using BOLD physiological correction described in section 2.3.1. In addition, measured (a) cardiac and (b) respiratory signals that are down-sampled to 4 Hz are shown.

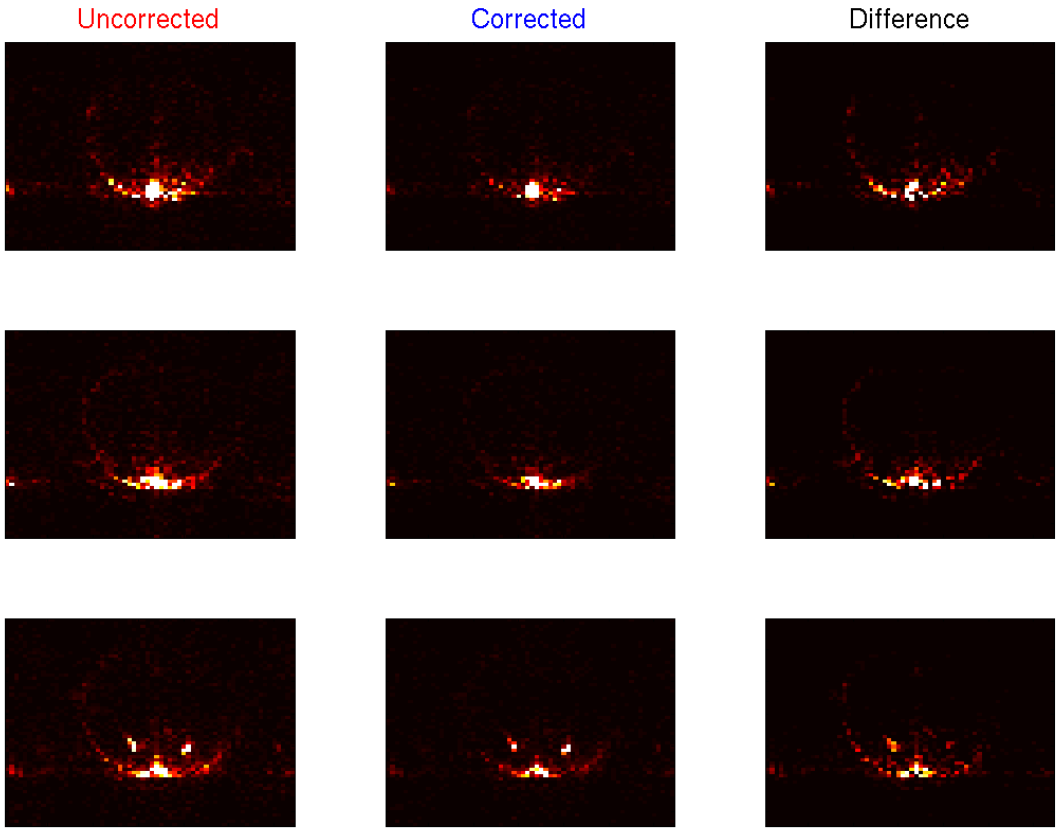

Figure 6. Data for BOLD images acquired at a TR of 250 ms. Image intensity corresponds to the sum of the Fourier spectrum over a frequency band that encompasses the respiratory peak frequency ($0.3 \pm 0.05 Hz$). Column 1 shows the uncorrected data, column 2 shows the corrected data, and column 3 shows the difference between the two. Each row corresponds to data from one slice (slices 1 to 3). All images are scaled equally.

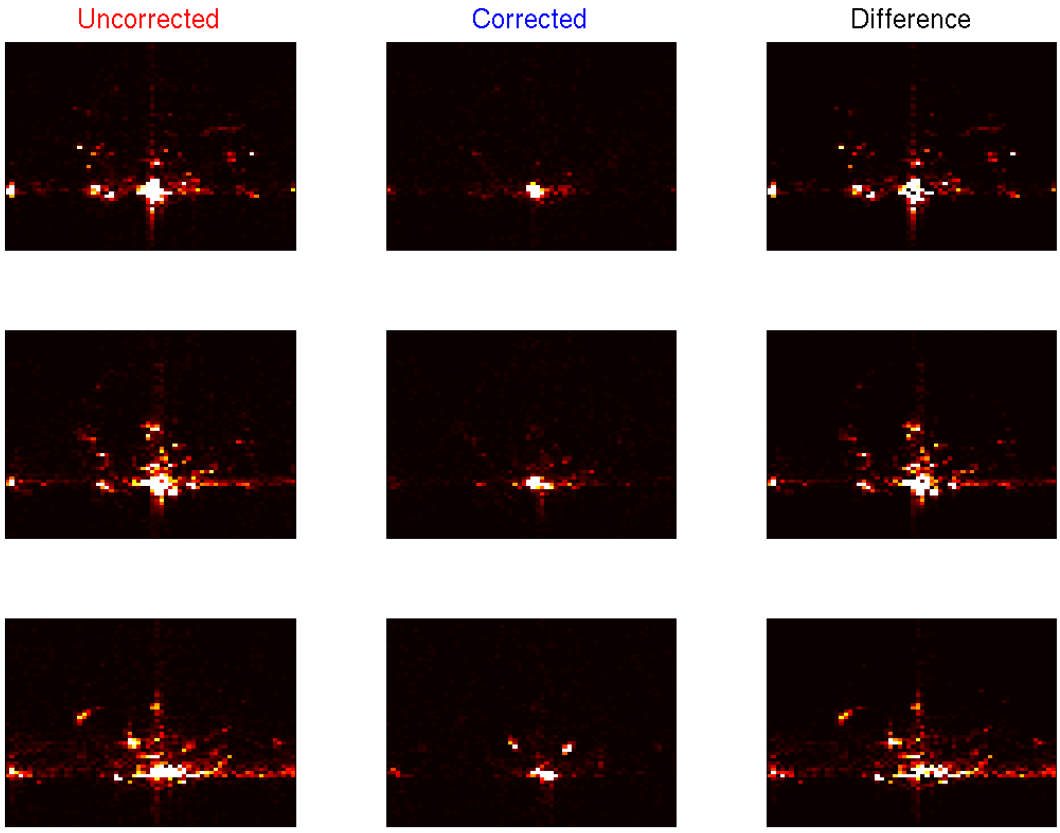

Figure 7. Data for BOLD images acquired at a TR of 250 ms. Image intensity corresponds to the sum of the Fourier spectrum over a frequency band that encompasses the cardiac peak frequency ($0.9 \pm 0.05 Hz$). Column 1 shows the uncorrected data, column 2 shows the corrected data, and column 3 shows the difference between the two. Each row corresponds to data from one slice (slices 1 to 3). All images are scaled equally.

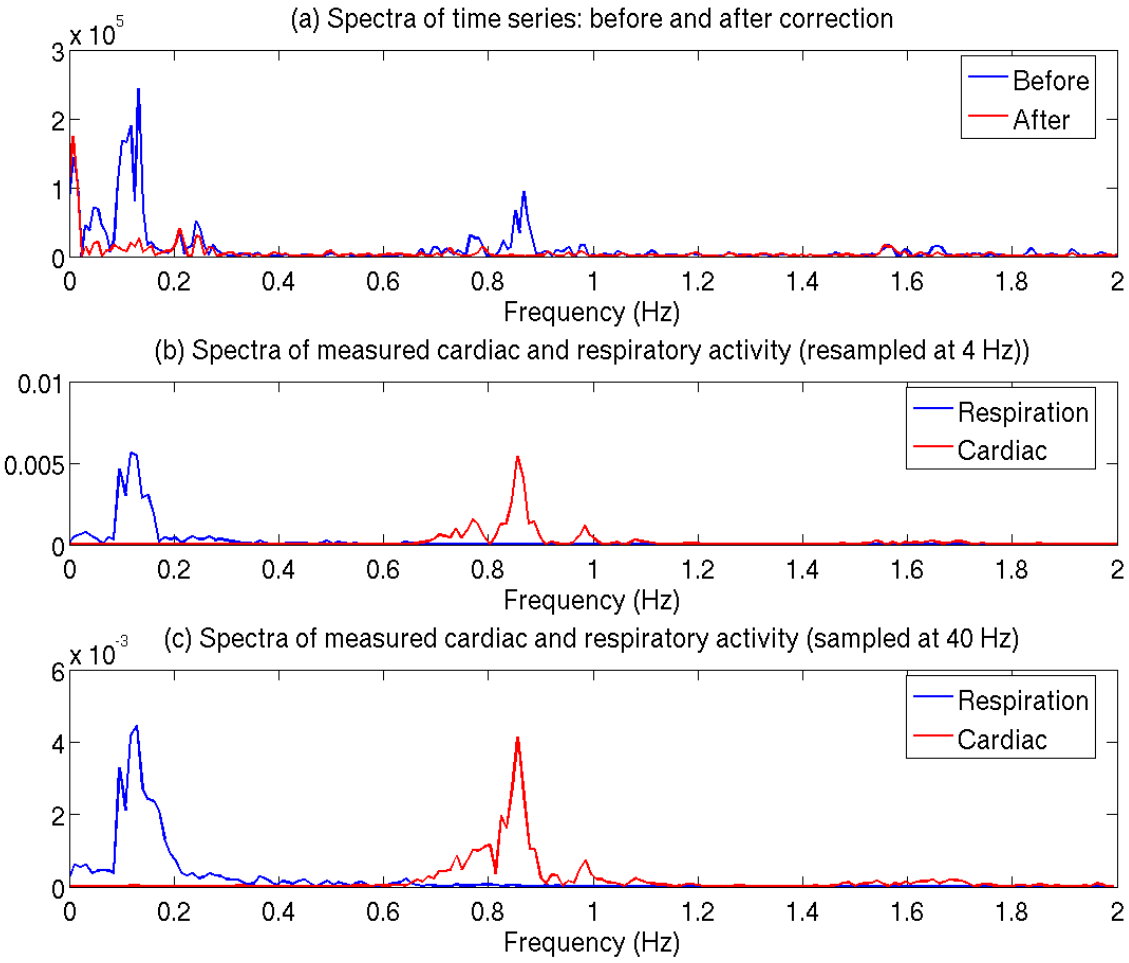

Figure 8. Fourier spectra of a single voxel (BOLD, TR = 250ms). (a) Spectra before and after noise correction. (b) Spectra of the physiological data resampled to the image sample frequency. (c) Spectra of the physiological data at the original sampling frequency of 40 Hz.

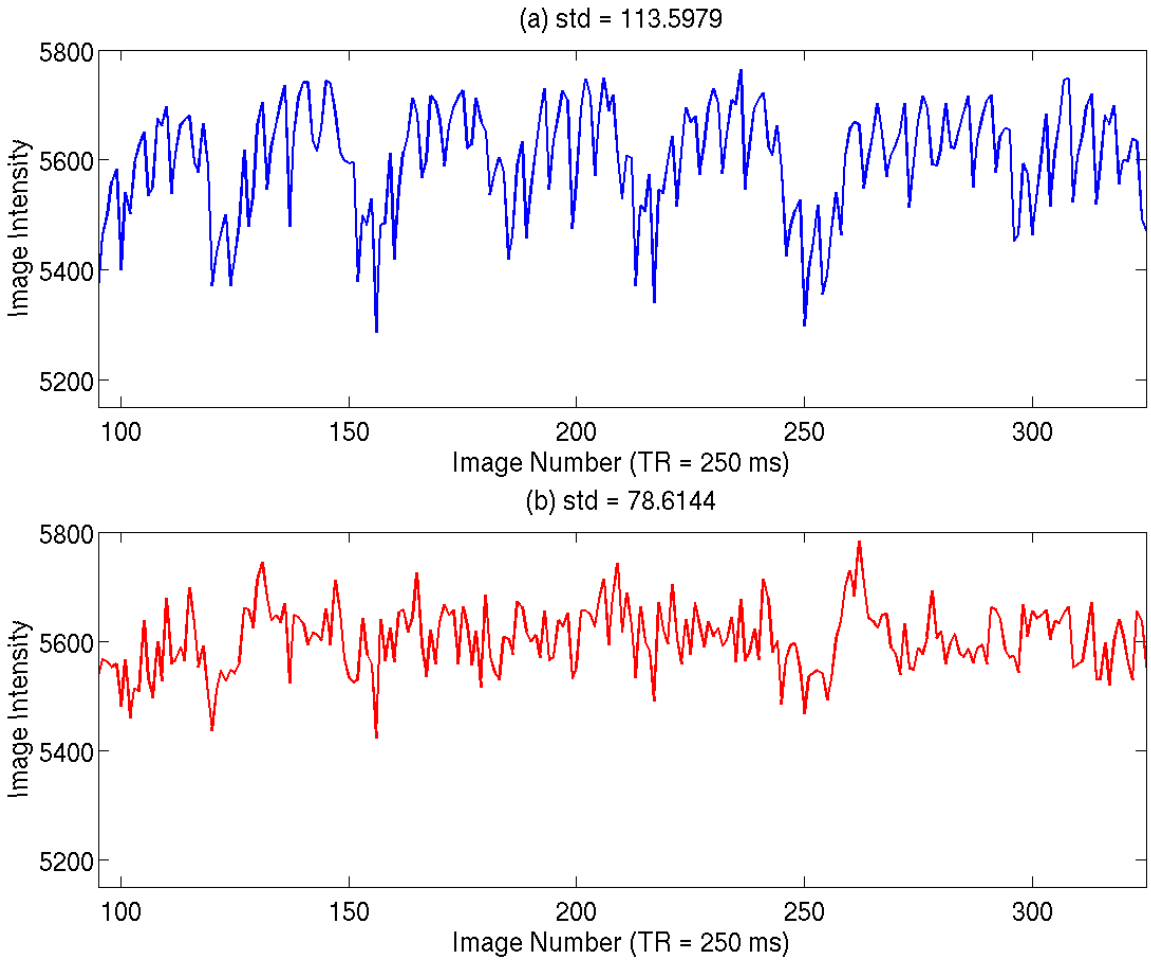

Figure 9. Example of resting-state (BOLD, TR = 250 ms) time series (a) before and (b) after correction. The standard deviation of each time series is also shown.

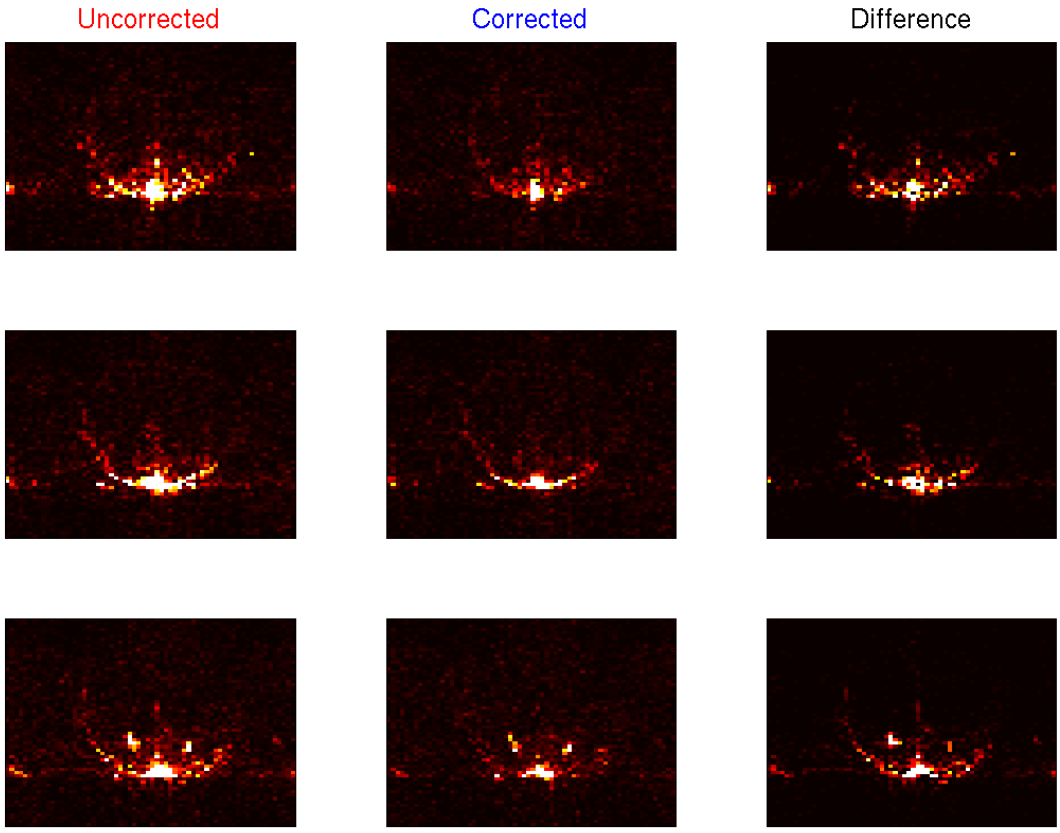

Figure 10. Data for BOLD images resampled to a TR of 2000 ms. Image intensity corresponds to the sum of the Fourier spectrum over a frequency band that encompasses the respiratory peak frequency and aliased cardiac peak frequency ($0.3 \pm 0.05 Hz$). Column 1 shows the uncorrected data, column 2 shows the corrected data, and column 3 shows the difference between the two. Each row corresponds to data from one slice (slices 1 to 3). All images are scaled equally.

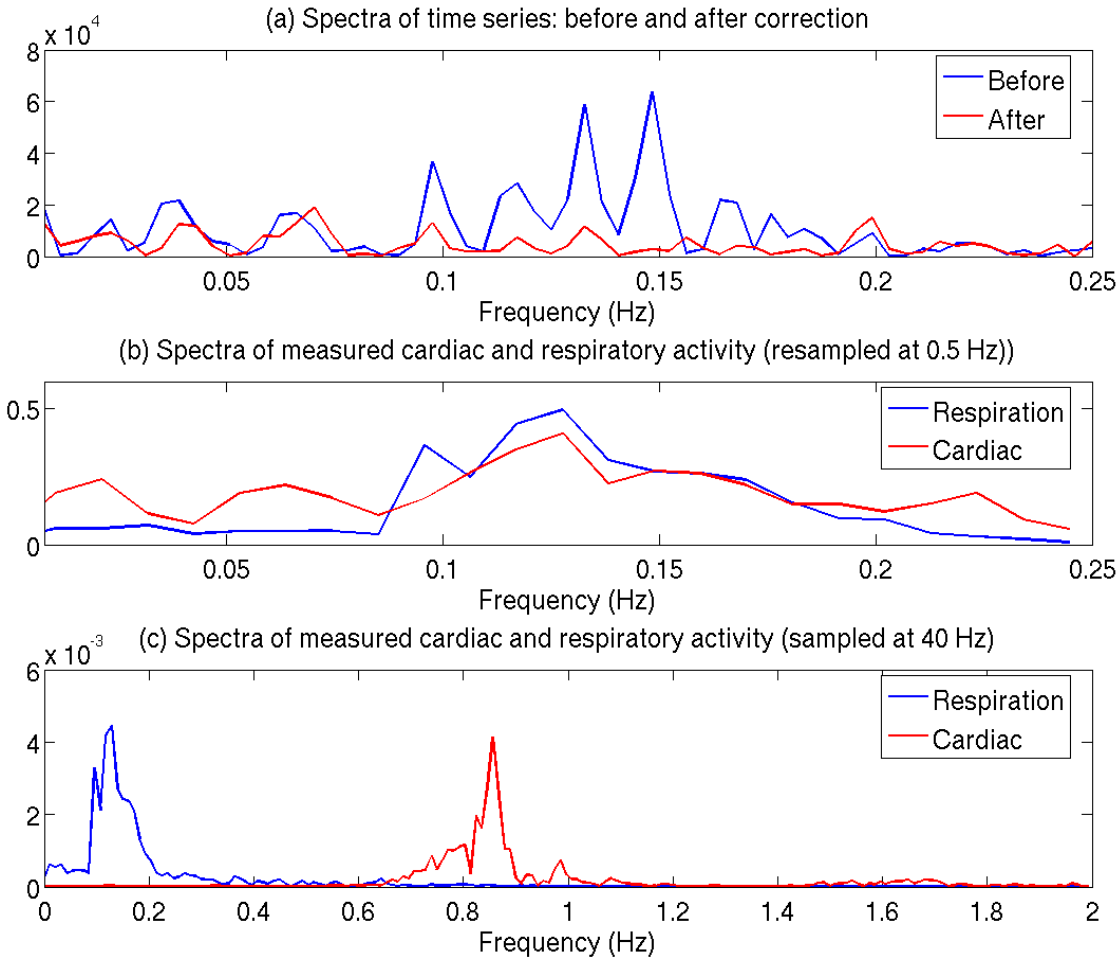

Figure 11. Fourier spectra of a single voxel (BOLD, TR = 2000ms). (a) Spectra before and after noise correction. (b) Spectra of the physiological data resampled to the image sample frequency. (c) Spectra of the physiological data at the original sampling frequency of 40 Hz.

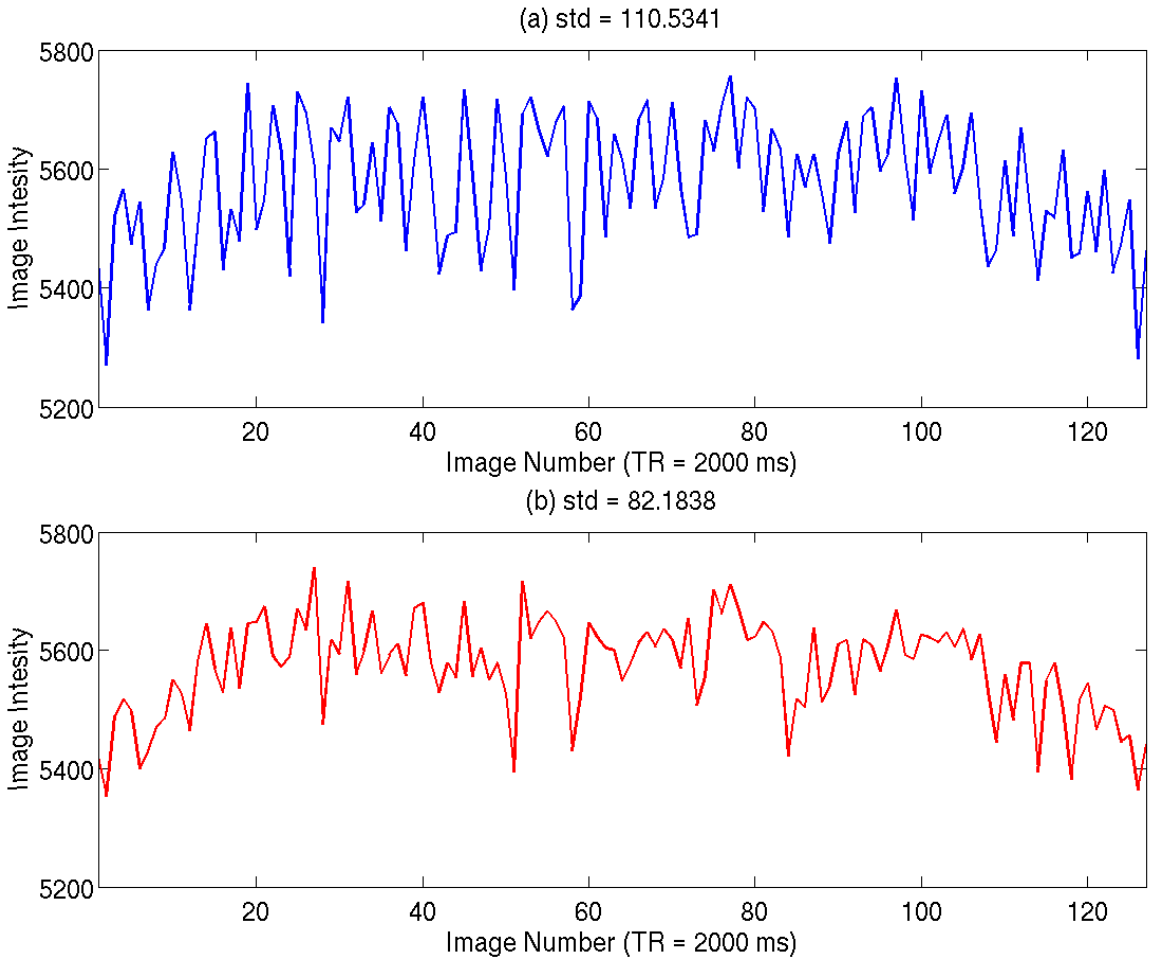

Figure 12. Example of resting-state (BOLD, TR = 2000 ms) time series (a) before and (b) after correction. The standard deviation of each time series is also shown.

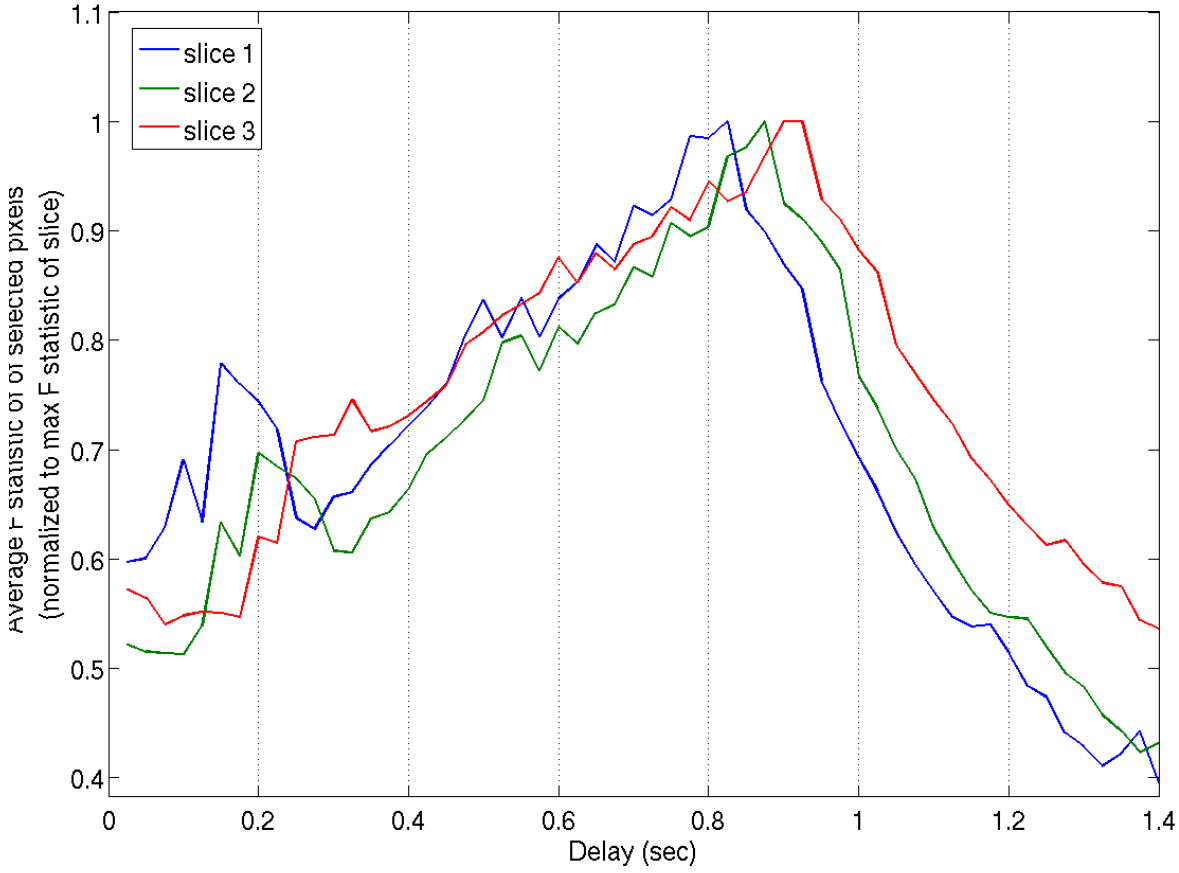

Figure 13. F statistic versus delay time. The average F statistic of all voxels that exceed the threshold F statistic corresponding to a p value of 0.05 is shown. Plots are normalized to maximum F statistic of each slice. Average F statistic peaks at delay times of 850 ms, 900 ms and 950 ms for slices 1, 2, and 3, respectively. Data shown here are for subject 1.

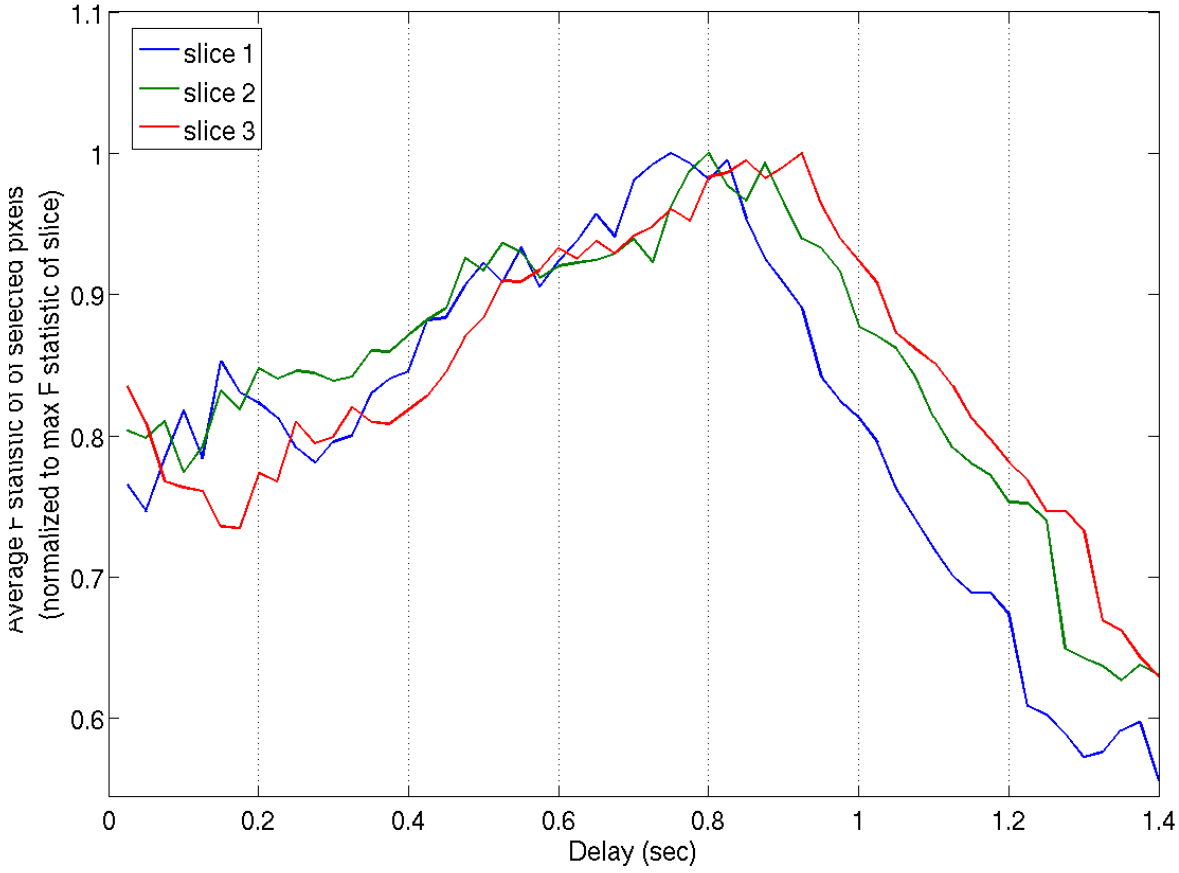

Figure 14. F-statistic versus delay for selected voxels from all subjects. The average F statistic of all voxels that exceed the threshold F statistic corresponding to a p value of 0.05 is shown. Plots are normalized to max F statistic of each slice. Average F statistic peaks at delay times of 750 ms, 800 ms and 925 ms for slices 1, 2, and 3, respectively.

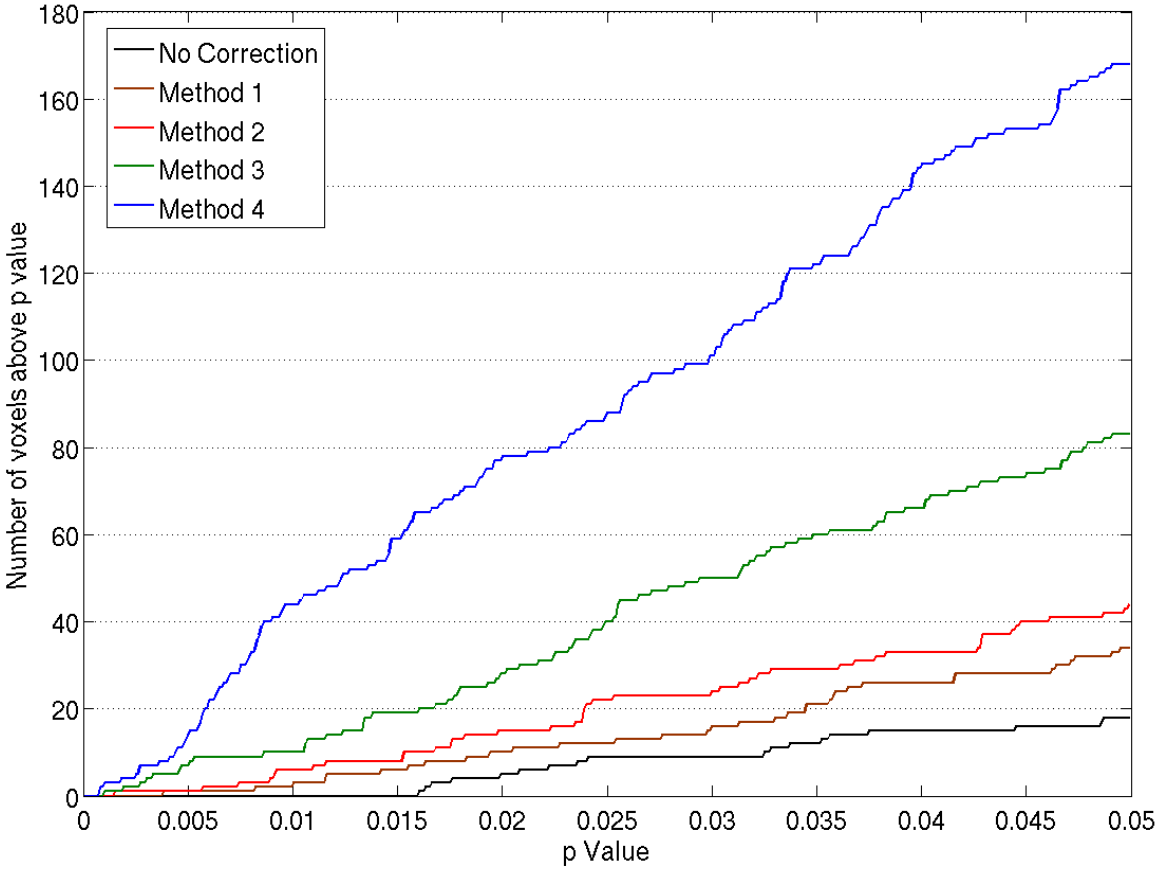

Figure 15. Average number of voxels for subject 1 that exhibit an F statistic above a specified threshold. p-values corresponding to thresholds range from 0.0 to 0.05.

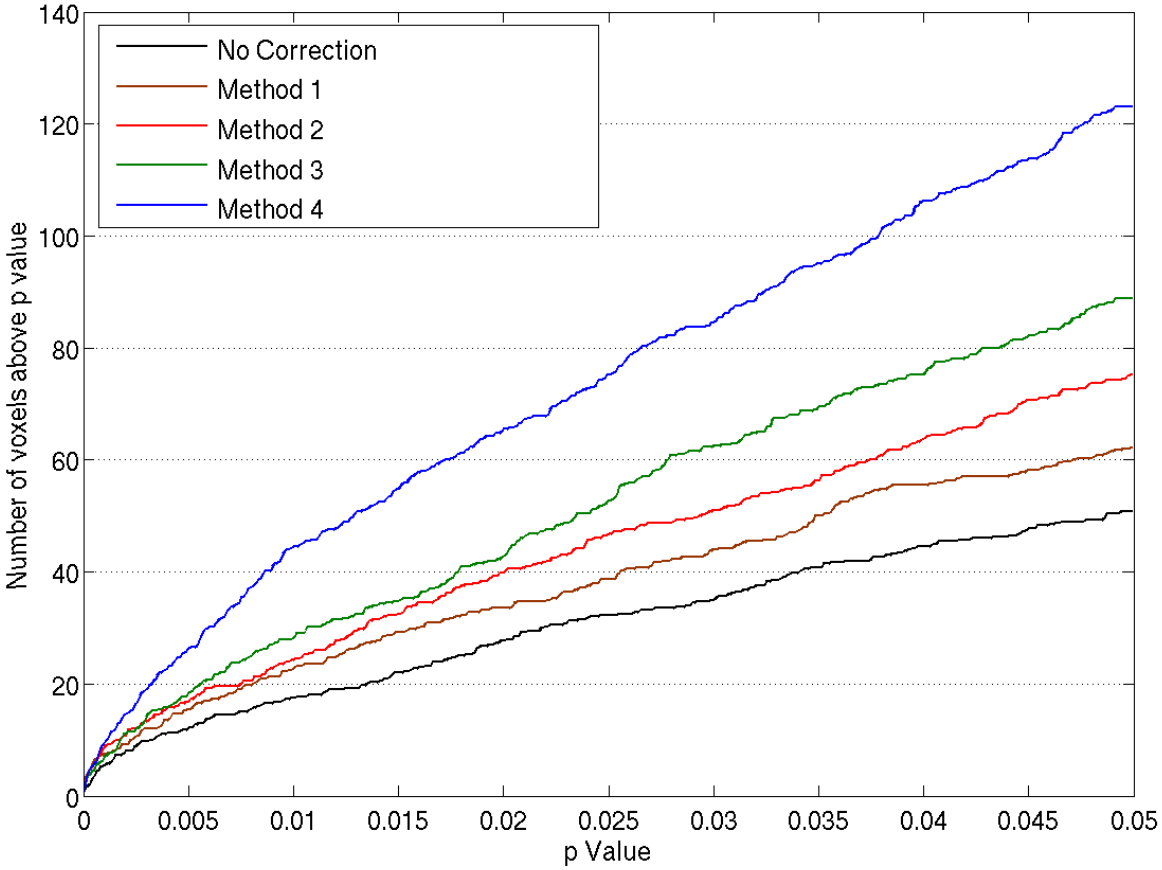

Figure 16. Average number of voxels across all subjects that exhibit an F statistic above a specified threshold. p-values corresponding to thresholds range from 0.0 to 0.05.

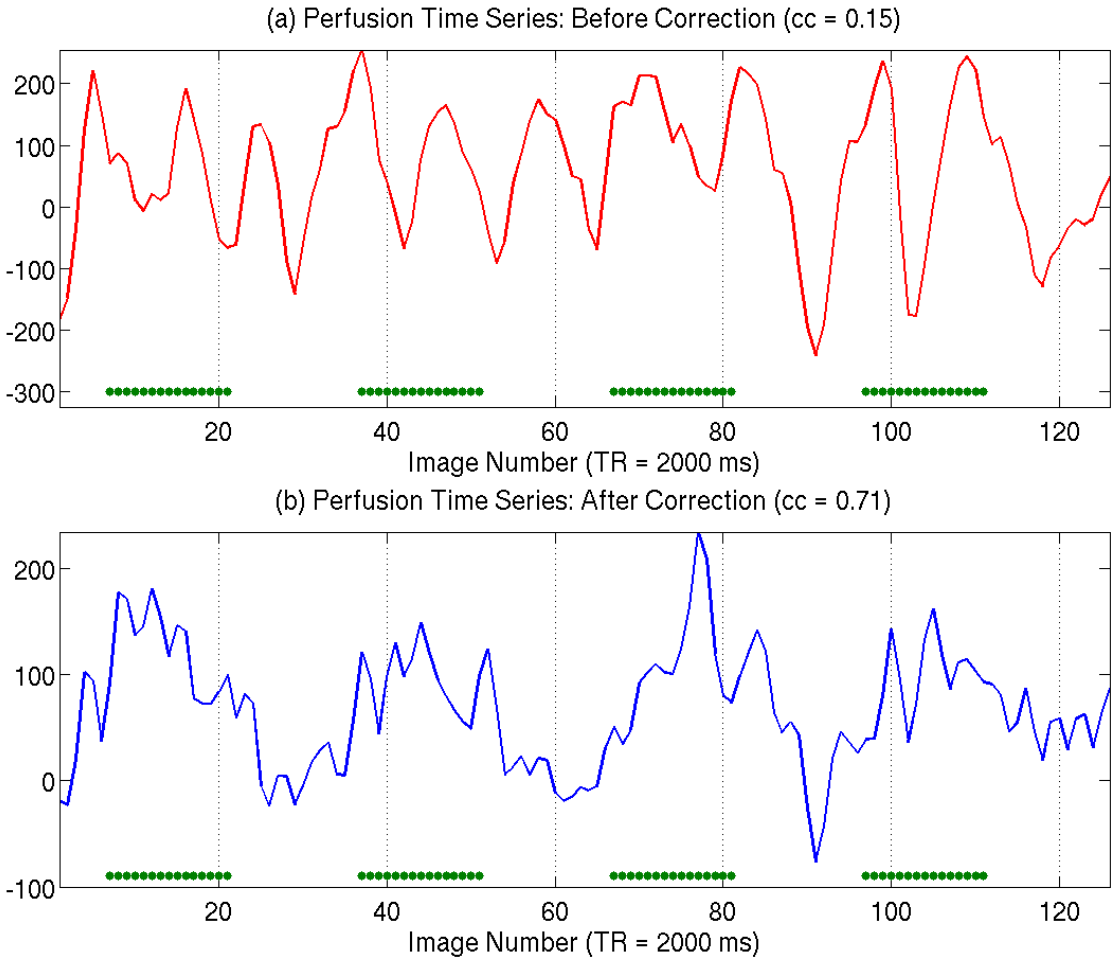

Figure 17. Example of a perfusion time series (a) before and (b) after correction (method 4) for subject 1. Green dotted line denotes time during which the stimulus was shown to the subject.

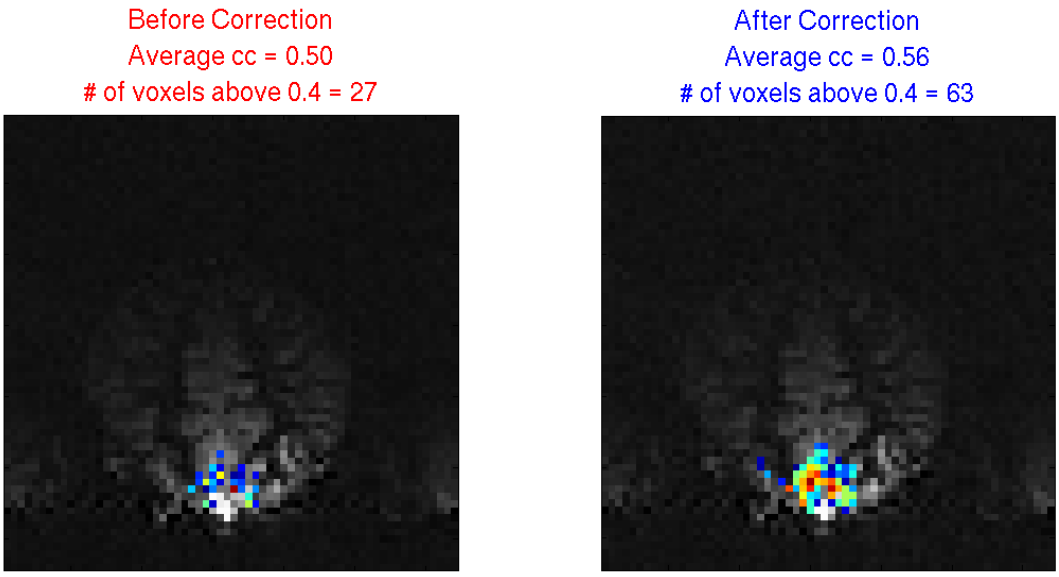

Figure 18. Example of a correlation map overlaid on an average perfusion map for subject 1. Results are shown before and after correction (method 4). Average cc and number of voxels above a threshold of 0.4 are summarized below each map.

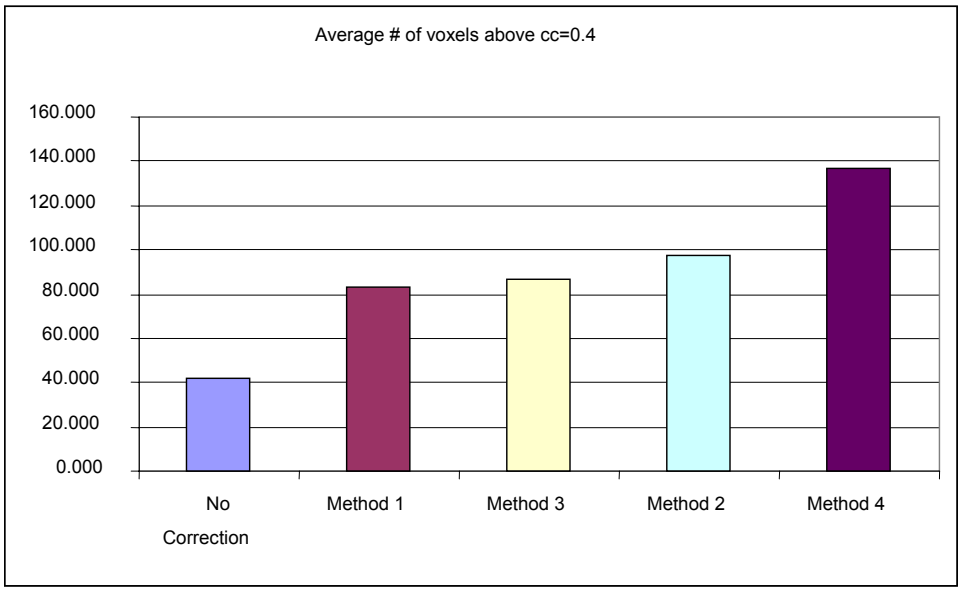

Figure 19. Average number of voxels that exceed a correlation threshold of 0.4 across all subjects. Results are shown for no correction and correction with methods 1 – 4.

REFERENCES

Buxton, R. B. (2002). Introduction to Functional Magnetic Resonance Imaging. Cambridge, Press Syndicate for the University of Cambridge.

Cox, R. W. (1996). "AFNI: software for analysis and visualization of functional magnetic resonance neuroimages." Comput Biomed Res **29**(3): 162-73.

Dagli, M. S., J. E. Ingeholm, et al. (1999). "Localization of cardiac-induced signal change in fMRI." Neuroimage **9**(4): 407-15.

Detre, J. A., J. S. Leigh, et al. (1992). "Perfusion imaging." Magn Reson Med **23**(1): 37-45.

Frank, L. R., R. B. Buxton, et al. (2001). "Estimation of respiration-induced noise fluctuations from undersampled multislice fMRI data." Magn Reson Med **45**(4): 635-44.

Glover, G. H., T. Q. Li, et al. (2000). "Image-based method for retrospective correction of physiological motion effects in fMRI: RETROICOR." Magn Reson Med **44**(1): 162-7.

Hu, X., T. H. Le, et al. (1995). "Retrospective estimation and correction of physiological fluctuation in functional MRI." Magn Reson Med **34**(2): 201-12.

Liu, T. T., L. R. Frank, et al. (2001). "Detection power, estimation efficiency, and predictability in event-related fMRI." Neuroimage **13**(4): 759-73.

Liu, T. T., E. C. Wong, et al. (2002). "Analysis and design of perfusion-based event-related fMRI experiments." Neuroimage **16**(1): 269-82.

Luh, W. M., E. C. Wong, et al. (2000). "Comparison of simultaneously measured perfusion and BOLD signal increases during brain activation with T(1)-based tissue identification." Magn Reson Med **44**(1): 137-43.

Noll, D. C. and W. Schneider (1994). "Theory, simulation, and compensation of physiological motion artifacts in functional MRI." IEEE International Conference on Imaging Processing, Austin, Texas: 40.

Pfeuffer, J., G. Adriany, et al. (2002). "Perfusion-based high-resolution functional imaging in the human brain at 7 Tesla." Magn Reson Med **47**(5): 903-11.

Pfeuffer, J., P. F. Van de Moortele, et al. (2002). "Correction of physiologically induced global off-resonance effects in dynamic echo-planar and spiral functional imaging." Magn Reson Med **47**(2): 344-53.

Restom, K., Y. Behzadi, et al. (2004). Image based physiological noise correction for perfusion-based fMRI. Twelfth Meeting, International Society for Magnetic Resonance in Medicine, Kyoto, Japan.

Turner, R., P. Jezzard, et al. (1993). "Functional mapping of the human visual cortex at 4 and 1.5 tesla using deoxygenation contrast EPI." Magn Reson Med **29**(2): 277-9.

Wong, E. C., R. B. Buxton, et al. (1997). "Implementation of quantitative perfusion imaging techniques for functional brain mapping using pulsed arterial spin labeling." NMR Biomed **10**(4-5): 237-49.

Wong, E. C., R. B. Buxton, et al. (1998). "Quantitative imaging of perfusion using a single subtraction (QUIPSS and QUIPSS II)." Magn Reson Med **39**(5): 702-8.